Fibroblast autofluorescence in connective tissue disorders: a future tool for clinical and differential diagnosis?

Monica Monici
University of Florence
Department of Clinical Physiopathology
ASAcampus, ASA Research Division
Florence, Italy

Venere Basile
Giovanni Romano
University of Florence
Department of Clinical Physiopathology
Medical Physics Unit
Florence, Italy

Lucia Evangelisti
Laura Lucarini
Monica Attanasio
University of Florence
Department of Medical and Surgical Critical Care
and
Marfan Center
Azienda Ospedaliero-Universitaria Careggi, Florence
and
Center for the Study at Molecular and Clinical Level of
Chronic, Degenerative, and Neoplastic Diseases
to Develop Novel Therapies
Florence, Italy

Enrico Bertini
Bambino Gesù Pediatric Hospital IRCCS
Department of Laboratory Medicine
Unit of Molecular Medicine
Rome, Italy

Franco Fusi
University of Florence
Department of Clinical Physiopathology
Medical Physics Unit
Florence, Italy

Gian Franco Gensini
University of Florence
Department of Medical and Surgical Critical Care
and
Marfan Center
Azienda Ospedaliero-Universitaria Careggi, Florence
and
Center for the Study at Molecular and Clinical Level of
Chronic, Degenerative, and Neoplastic Diseases
to Develop Novel Therapies
Florence, Italy
and
Fondazione Don Carlo Gnocchi ONLUS
Centro S.Maria degli Ulivi-IRCCS
Florence, Italy

Guglielmina Pepe
University of Florence
Department of Medical and Surgical Critical Care
and
Marfan Center
Azienda Ospedaliero-Universitaria Careggi, Florence
and
Center for the Study at Molecular and Clinical Level of
Chronic, Degenerative, and Neoplastic Diseases
to Develop Novel Therapies
Florence, Italy

Abstract. Marfan syndrome (MFS) is an inherited disorder of connective tissue due to mutations in FBN1 (90%) and TGFBR1 and TGFBR2 (5 to 10%) genes. Clinical and differential diagnosis is difficult because of the inter- and intrafamiliar marked heterogeneity and the variable onset age of clinical manifestations. Among the disorders, in differential diagnosis, thoracic aortic aneurysm (TAA) and Ullrich scleroatonic muscular dystrophy (UCMD) are reported. We evaluate the possibility of utilizing autofluorescence (AF) analysis as a diagnostic tool in the clinical and/or differential diagnosis of MFS and related disorders and in the investigation of the molecular mechanisms involved. Both multispectral imaging autofluorescence microscopy (MIAM) and autofluorescence microspectroscopy (AMS) have been used to characterize AF emission of fibroblasts from patients affected by inherited connective tissue disorders. Our preliminary results show significant differences in AF emission between normal and pathological fibroblasts, suggesting possible improvement in diagnostics of connective tissue disorders by AF analysis. [DOI: 10.1117/1.2982533]

Keywords: fluorescence; microscopy; imaging; fluorescence spectroscopy; cells; biomedical optics.

Paper 08028R received Feb. 5, 2008; revised manuscript received May 11, 2008; accepted for publication May 15, 2008; published online Oct. 21, 2008.

1 Introduction

Marfan syndrome (MFS; OMIM #154700) is an inherited autosomal dominant disorder. Marfan syndrome (MFS) is a pleiotropic disease with multisystemic clinical manifestations. Among the disorders, in differential diagnosis, Ullrich scleroatonic muscular dystrophy (UCMD) and thoracic aortic aneurysm (TAA) are reported.

Fibrillin 1 is a 160 Kd extracellular matrix glycoprotein mainly made by multiple calcium-binding and noncalcium-binding EGF-like repeats. Mutations in the FBN1 gene are associated to MFS in about 90% of cases.[1] Recently, two other genes, TGFBR1[2,3] and TGFBR2,[4] have been demon-

Address all correspondence to: Monica Monici, ASAcampus, ASA Research Div., c/o Univ. of Florence, Dept. of Clinical Physiopathology, Florence, Italy; Fax: +39 055 4271413; E-mail: monica.monici@unifi.it

1083-3668/2008/13(5)/054025/8/$25.00 © 2008 SPIE

strated to be associated to MFS2, (#154705). Mutations in TGFBR2 were also found in patients with TAA.[5] TAA is more complicated, since FBN1 and TGFBR2 are both associated in about 5% of cases, but at least three other genes are involved.[6]

UCMD (#254090) is an autosomal recessive[7] or dominant[8] myopathy characterized by generalized neonatal muscle weakness, proximal joint contractures, and distal hyperlaxity. Both forms are caused by mutations in COL6A1, COL6A2 (chr. 21q22.3), and COL6A3 (chr. 2q37) genes that codify for the three chains (α1, α2, and α3) of collagen type VI, a ubiquitous extracellular matrix protein.[9]

In recent years, many imaging and ultramicroscopy techniques have been applied to the study of these disorders with the aim of identifying useful tools for both diagnostic approach and better understanding of the molecular pathophysiology of these diseases.[10] In this paper, we propose the application of multispectral imaging techniques based on autofluorescence (AF) analysis.

The term "autofluorescence" is used to distinguish the endogenous fluorescence of cells and tissues from the fluorescence obtained by treating specimens with exogenous fluorescent markers.[11] The potential use of cell and tissue AF for diagnostic purposes was already recognized at the beginning of the past century,[12] but only recently, the availability of high-sensitivity devices has allowed the easy detection of low-quantum yield AF signals.[13] Many studies have been performed on the application of AF-based techniques for discriminating pathological from physiological conditions in cells and tissues.[14]

The AF pattern is related to the morphological and functional state of the cells,[11,14,15] as demonstrated by investigations on cell energy metabolism,[16] and its changes in pathological conditions[17] as well as during pharmacological treatments.[18] Changes of the AF properties have been found in skin fibroblasts isolated from patients with neurological disorders; therefore, the possibility to utilize AF analysis as eq support for the diagnosis of these pathologies has been suggested.[19]

To the best of our knowledge, studies on AF analysis of fibroblasts from patients with connective tissue disorders are not reported in the literature. The aim of this work is to characterize the AF properties of fibroblasts derived from patients affected by inherited connective tissue diseases and to compare them with those of normal fibroblasts in order to evaluate the possibility of utilizing AF analysis as a diagnostic tool in the diagnosis and/or differential diagnosis of these disorders and in the investigation of the mechanisms involved in these pathological conditions.

2 Materials and Methods

2.1 *Multispectral Imaging Autofluorescence Microscopy (MIAM) and Autofluorescence Microspectroscopy (AMS)*

Multispectral imaging is the acquisition of spectrally resolved information at each pixel of an imaged scene. Many different technologies can be employed to generate such information, ranging from multiposition filter wheels, gratings and prisms, laser-scanning single-point spectrographs, electronically adjustable tunable filters, Fourier transform imaging spectrometry, and computed tomographic imaging spectroscopy (reviewed in Ref. 20).

Our technique is based on a band-sequential approach performed on a wide-field fluorescence microscope. Multiposition filter wheels are band-sequential filters that are coupled to the focal plane of a CCD. By sequentially inserting the filters and exposing the sensor, complete images are acquired band by band.

Fibroblast AF was analyzed by an inverted epifluorescence microscope (Nikon Eclipse TE2000-E) equipped with an oil-immersion CFI S Fluor 100× (NA 1.3) objective, under 365-nm excitation from a filtered (10-nm bandwidth interference filter, 365FS10-25, Andover Corp., Salem, New Hampshire) high-pressure mercury lamp (HBO 100 W, Osram, Germany). The excitation light intensity was reduced with neutral density filters. The fluorescence signal, transmitted through a dichroic mirror at 400 nm (DM400, Nikon), was detected, according to the position of a mobile mirror, by a Hires IV digital CCD camera (DTA, Pisa, Italy) equipped with a Kodak KAF261E detector (20 μm, 512×512 pixels), or by a spectrophotometer. This instrument is based on a polichromator (SpectraPro 500i ARC, Massachussets), connected to the microscope through an optical fiber bundle (1-mm diameter) and comprising a Hires III cooled digital CCD device (DTA) with a back-illuminated SITe sensor (330×1100 pixels). Hence, the system allowed sequential recording of images and spectra from each cell examined in order to get information about emission intensity and fluorophore spectral and spatial distribution.

Fluorescence imaging was accomplished using a motorized filter wheel, containing up to 8 different interference filters, placed in front of the CCD detector. This allowed a multispectral sequential acquisition in different emission bands. The choice of the filter combination was made on the basis of the main spectral bands determined by preliminary analysis of the AF spectra. Both the CCD camera and the filter wheel were controlled by a modified routine running under Visa software (DTA).

Fluorescence images were directly digitized in the CCD controller with a 16-bit dynamics and transferred to the storage computer on a digital interface. The size of the field detected by the 100× objective was about 69×69 μm (spatial calibration of 0.13 μm pixel^{-1}), as determined by imaging 6-μm fluorescent microspheres (Molecular Probes, Leiden, The Netherlands).

For each sample, three 40-nm-wide (FWHM) spectral bands, peaked at about 450, 550, and 650 nm (450 FS 40-25, 550 FS 40-25, and 650 FS 40-25, respectively, Andover, Salem, New Hampshire), were used in order to sequentially acquire three fluorescence images with the same integration time. The overall acquisition was no longer than 3 s. Monochrome images were then combined in a single multicolor image using the RGB technique. The multicolor images were obtained by the Image Combine Channels algorithm of Image Pro-Plus 4.5.1 (Media Cybernetics, Inc., Silver Springs, Maryland), after the identification of the three grayscale images (acquired at 650, 550, and 450 nm, respectively) with the RGB components. RGB color images were synthesized from the spectral data into those color channels. All the images identified as RGB images in this report are derived from

the spectral data sets and not from conventional color sensors.

Fluorescence spectra were recorded over a spot of about 10 μm in diameter, as estimated by using 6-μm fluorescent microspheres (F-14808, Molecular Probes). Fluorescence spectra, recorded with a 2 to 4 s integration time, were corrected for the optical system spectral response and smoothed by a Gaussian convolution algorithm.

Both spectra and multispectral images were detected on single cells. Three different slides were prepared from each sample. At least 30 cells per slide were scored in 10 random fields/slide. Therefore, AF spectra were calculated as an average from at least 30 different cells.

The characterization of fibroblast AF was performed by two sets of experiments:

- In the former, we studied the relationship between cell AF and culture state both in normal and pathological fibroblasts.
- In the latter, we analyzed the differences between control fibroblasts and those from patients affected by connective tissue disorders.

2.2 *Patient and Control Recruitment*

We analyzed seven patients, two affected by UCMD, two by TAA, and three by MFS, one of them with a particularly by severe cardiovascular involvement.

2.3 *Skin Biopsies and Establishment of Primary Cultures of Dermal Fibroblasts*

Skin biopsies were obtained from patients and healthy volunteers. Primary fibroblasts were grown from skin biopsies as described.[21,22] All reagents were obtained from GIBCO BRL (Life Technologies, United Kingdom).

3 Results and Discussion

3.1 *Comparison of Multispectral Fluorescence Imaging Techniques*

Unlike some other techniques, for example, those that use prisms or gratings to disperse and collect all wavelengths simultaneously, this design allows the user to vary the exposure time as a function of wavelength, thus optimizing signal-to-noise in situations where sensitivity varies over the spectral range. Moreover, the wavelengths acquired can be arbitrarily spaced through the spectral range of interest, allowing the user to maximize signal-to-noise by acquiring only the most informative bands. Other advantages include excellent optical properties yielding near-diffraction-limited images, spectral stability to a nanometer, and high reliability.

As always, there are also some disadvantages related to band-sequential approaches in general and/or multiposition filter wheels in particular. A band-sequential approach implies that the complete image stack is built up over time thus, if significant sample or camera movement occurs during the acquisition image quality is reduced. Also, photobleaching during acquisition can be a concern, since some wavelengths will be acquired after others, and therefore will be subject to longer illumination before being detected.

Band-sequential approaches, can be performed also by using liquid-crystal tunable filters. This technique has the advantage of the absence of moving parts but the disadvantage of lower light throughput; transmission efficiencies are typically in the 30% range, in comparison to traditional interference filters that can transmit 80% of incoming light.

Laser scanning confocal microscopy rasters a laser spot across the object, obtaining a full image one point at a time, and requires brighter illumination to generate an image of the same brightness as that using wide-field fluorescence microscopy, due to the pinhole rejection of out-of-focus light. Additional light losses arise from the greater number of reflective and refractive surfaces in the scan generators of confocal microscopy. Moreover, the AF signal is very low, and the cooled CCD camera has detection efficiency 1.5 to 4 times higher than that of the photomultiplier tubes (PMTs) of the laser-scanning confocal microscope. This means that there is an important decrease in the number of photons detected, so confocal specimens may be vulnerable to photobleaching and photo damage. The use of a multiphoton technique is probably the best choice from a scientific point of view. The specimen above and below the plane of focus is subjected merely to IR light that causes photodamage. The peak amplitude of the IR pulses is large, but the mean power of the beam is only a few tens of milliwatts, not enough to cause substantial heating of the specimen. Disadvantages of multiphoton imaging include the need for a high-peak-power, pulsed laser and, until now, the lack of high-performance optical filters that provide sufficient throughput across the whole emission range of interest and sufficient blocking across the full laser tuning range.

3.2 *Patients*

We analyzed seven patients, indicated as UCMD1, UCMD2, TAA1, TAA2, MFS1, MFS2, and MFS3. (This last patient presents enlargement of the entire aorta and particularly severe cardiovascular progression.) All patients are males except for MFS1, who is a female.

UCMD1 (1 year old) and UCMD2 (3 years old) clinical phenotypes and molecular data are reported by Camacho et al.[7]

TAA 1 (38 years old) and TAA2 (40 years old) both underwent aortic surgery for thoracic aortic dissection at ages 36 and 38, respectively. They presented mild skeletal manifestations such as pectus carenatum, kyphosis, and pes planus (TAA1), and pectus carenatum, scoliosis, and arachnodactily (TAA2).

MFS1 (34 years old) presented the involvement of the skeleton (altered upper-lower segment ratio, severe kyphoscoliosis, reduced extension at the elbows, and positive thumb and wrist signs) and cardiovascular (thoracic aortic dissection) and central nervous (mild dural ectasia) systems as major criteria and eye (myopia) and skin (striae distensae) as minor criteria. MFS2 (31 years old) was affected by ectopia lentis and thoracic aortic dilatation as major criteria and pectus excavatum, moderate kyphoscoliosis, and striae distense as minor criteria. MFS3 (40 years old) was affected by enlargement of the entire aorta (he underwent cardiovascular surgery at the age of 24 for thoracic aortic dissection), pectus excavatum, severe scoliosis, positive wrist sign and pes planus as major criteria and striae distense as a minor criterion according to De Paepe et al.[23]

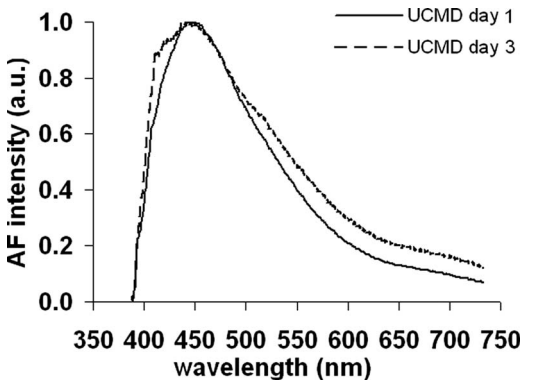

Fig. 1 AF spectra for UCMD cell populations, analyzed at day 1 and day 3 after thawing.

3.3 *Molecular Analysis*

UCMD1 was homozygous for a one-nucleotide insertion in the COL6A2 gene, while UCMD2 was a genetic compound for heterozygous single-nucleotide substitutions in the COL6A2 gene, both affecting mRNA splicing.[7]

TAA1 and TAA2 were analyzed for mutations in FBN1, TGFBR1, and TGFBR2, but no mutations were detected.

MFS1 and MFS2 presented two missense mutations in exons 16 and 18 in the FBN1 gene, while MFS3 showed an insertion of two nucleotides at the end of FBN1.

3.4 *Preliminary Studies on the Relationship Between Cell AF and Culture State*

First, we set methodological aspects in order to avoid alteration of the results and to standardize protocols for future studies and diagnostic applications. Cell AF depends on the number of culture passages[15] and culture state: it is lower in freshly thawed cultures and increases as cells enter the exponential phase of growth to a maximum value with raised cell numbers.[24] Therefore, we investigated AF emission in normal and pathological fibroblasts as a function of the number of passages and time after thawing.

We assessed that no significant changes occurred in cell AF within five passages. For number of subculture passages >5, both AF intensity and spectral shape changed (data not shown). Moreover, we found significant variations in AF according to the time elapsed between thawing and AF analysis (Fig. 1).

For the longer time elapsed, the AF spectrum broadened toward the red. In order to understand the biochemical roots of this change, we calculated the value of the AF intensity ratios 445 nm/465 nm (indicated as 445/465), 445/520, 465/520, and 520/600, where the considered wavelengths (445, 465, 520, and 600 nm) correspond to the peaks of NAD(P)H bound, NAD(P)H free, oxidized flavins, and lipopigments, respectively. The results, reported in Table 1, show that the ratio 445/465, and consequently the equilibrium NAD(P)H bound/NAD(P)H free, did not change significantly. On the contrary, the ratios 445/520, 465/520, and 520/600 significantly decreased, suggesting an increase in oxidized flavins and lipopigments. Similar results were obtained analyzing fibroblasts from patients affected with other connective tissue disorders and from healthy donors. The increase in oxidized flavins and lipopigment content suggests an enhanced aerobic component of the energy metabolism and accumulation of oxidized products. Lipofuscin accumulation in proliferating fibroblasts *in vitro* has been already described by Sitte et al.[25]

Table 1 AF intensity ratios for UCMD cell populations, analyzed at day 1 and day 3 after thawing.

Ratio (wavelength, nm)	UCMD Day 1	UCMD Day 3
445/465	1.06±0.02	1.06±0.02
445/520	1.73±0.05	1.53±0.13
465/520	1.64±0.06	1.44±0.09
520/600	2.70±0.15	2.15±0.15

In summary, in agreement with other authors,[15,24] our findings ascertained that the number of passages as well as the time elapsing from thawing to AF analysis can influence cell AF emission, which is in turn related with proliferative activity and metabolic engagement of cells.

From these results, it is clear that suitable knowledge about the relationship between cell culture state and cell AF is required for developing AF-based techniques for diagnostic applications. The number of passages and time lag from thawing to analysis should be strictly controlled and, most important, should be the same for all the samples considered.

3.5 *Characterization of AF Emission in Normal and Pathologic Fibroblasts*

Following the findings described earlier, we utilized normal and pathological cells between passages 4 to 7 and compared samples with the same time elapsing after thawing.

The AF emission of fibroblasts collected from patients affected by connective diseases differed significantly from the emission of normal fibroblasts. Moreover, among the three diseases considered, i.e., MFS, UCMD, and TAA, different features have been observed.

Figure 2 shows some examples of AF patterns from normal (a) and pathological [(b) to (d)] cell populations. In normal fibroblasts, the AF mostly arose from cytoplasmic organelles while the nucleus was generally nonfluorescent, as expected under 365-nm excitation.[14] The AF emission was characterized by a blue component, whose distribution tallied that of mitochondria, and by a green-yellow component mostly located into granulations particularly abundant in the perinuclear area.

In fibroblast cultures from TAA patients (b), many cells were spindle-shaped and showed a homogeneously distributed blue-green fluorescence superimposed on the emission arising from the organelles. A similar pattern was observed in fibroblasts from UCMD patients (c). In these cells, the green-yellow fluorescent granules were also located in the peripheral area.

Fibroblasts from MFS patients (d) showed an increase in the fluorescent granules, whose emission appeared white, and a decrease in the blue component bound to the mitochondria. These changes were particularly marked in MFS3 (Fig. 3).

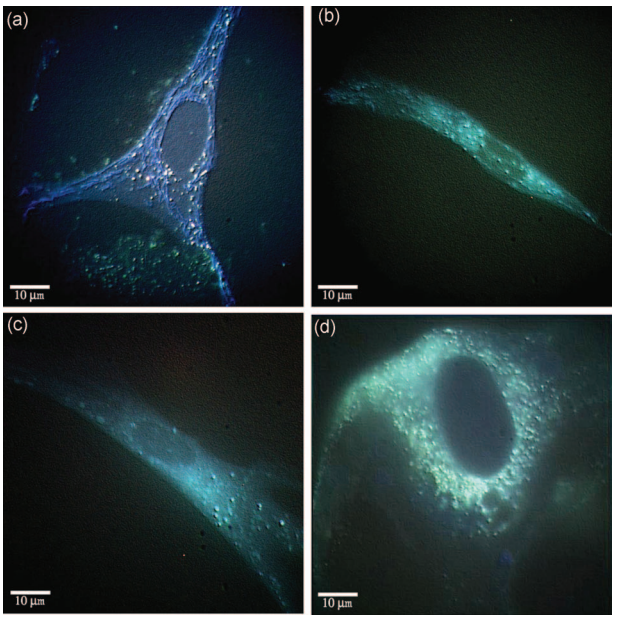

Fig. 2 AF pattern of control and pathological fibroblasts (a) control, (b) TAA, (c) UCMD, and (d) classical MFS. RGB color representation has been used (see Sec. 2).

Comparing the AF images of the three different connective diseases considered and controls, evident differences in cell shape can be noticed. In both TAA and UCMD, many cells appeared much elongated, while in MFS, the cells were roughly round shaped and more spread than in normal samples. It is known that cell shape represents a visual manifestation of an underlying balance of mechanical forces due to the cytoskeleton components and points of interaction between cell and substrate.[26] Thus, the different shapes exhibited by pathological fibroblasts could be the expression of changes in cytoskeleton organization, distribution of cell-matrix adhesions, and interactions with molecules of the extracellular matrix.

AMS revealed that the spectra of pathological fibroblasts differed from the normal ones for both emission intensity and spectral shape. TAA [Fig. 4(a)] and UCMD [Fig. 4(b)] showed a higher emission intensity (about 50% more), a slight blue shift of the maximum (7 nm), and a narrower spectrum. The comparison of the AF intensity ratios (Table 2) supplied information on variations in the content of endogenous fluorophores and relative balance among the different coenzyme pools. The value of the 445/465 ratio did not change appreciably. The 445/520 and 465/520 ratios increased significantly, suggesting that in pathological cells, the oxidized flavins decreased compared to the NAD(P)H. The ratio 445/600 increased too, indicating a decrease in the content of oxidation products like lipopigments, while the ratio 520/600 did not change significantly, in agreement with a decrease in both oxidized flavins and lipopigments.

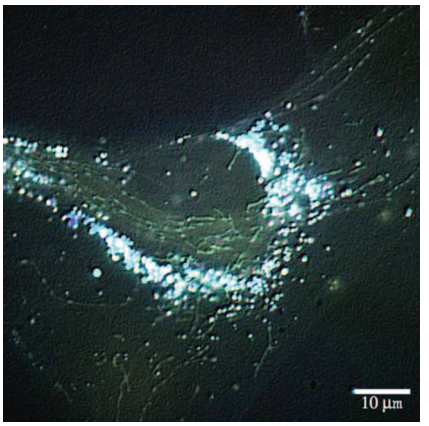

Fig. 3 AF pattern of MFS3 fibroblast. RGB color representation has been used (see Sec. 2).

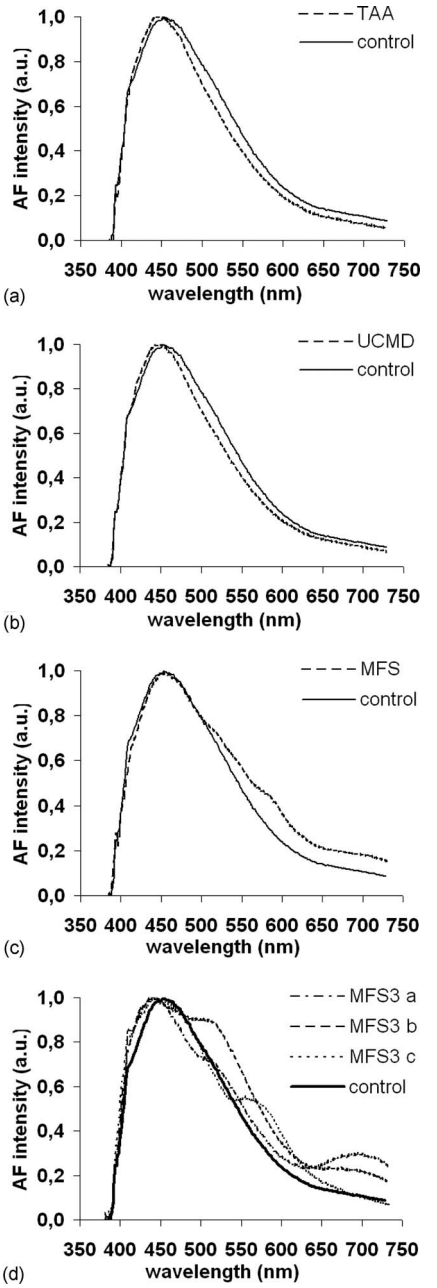

Fig. 4 AF spectra from different cell populations (a) TAA, (b) UCMD, (c) classical MFS, and (d) MFS3.

Table 2 AF intensity ratios for control, UCMD, TAA, and classical MFS.

Ratio (wavelength, nm)	Control	UCMD	TAA	MFS
445/465	1.01±0.04	1.05±0.02	1.05±0.03	1.00±0.03
445/520	1.45±0.15	1.69±0.07	1.75±0.15	1.36±0.06
465/520	1.45±0.08	1.62±0.06	1.65±0.1	1.36±0.05
445/600	4.0±0.5	4.7±0.3	4.6±0.5	2.7±0.3
520/600	2.7±0.15	2.80±0.15	2.90±0.35	2.0±0.2

Therefore, both AF imaging and spectral analysis indicated an impairment of cell energy metabolism in pathological fibroblasts. The AF pattern of the controls showed a rich network of filamentous mitochondria with radial distribution toward the cell periphery, intensely blue-fluorescent under 365-nm excitation. In pathological fibroblasts, we found a minor content of mitochondria, with a random distribution. The spectra of both TAA and UCMD fibroblasts showed an increase in total emission intensity together with an accumulation of NAD(P)H and depletion of oxidized flavins. This condition, together with paucity of mitochondria, is a typical characteristic of cells in which the anaerobic component of energy metabolism is enhanced. A higher anaerobic metabolism has been described in neoplastic cells, in fibroblasts from a stabilized cell line (high subculture passage) and from a transformed one.[15]

As regards fibroblasts from MFS patients, the spectral analysis showed a broadening toward the red, in comparison with controls. Moreover, in patients MFS1 and MFS2, the AF spectrum presented two shoulders at about 520 nm and 565 nm, respectively, and a peak of lower intensity at about 700 nm [Fig. 4(c)]. Patient MFS3, the one with the most severe symptoms, revealed a very complex situation: at least three subpopulations could be distinguished on the basis of the spectral characteristics and showed great variability in the spectral shape. For this reason, we decided to report three means representing as many cell subpopulations. Anyway, in all the cases, in addition to the principal peak (~445 nm), we found a pronounced shoulder at 520 or at 565 nm, and sometimes a third one at 700 nm [Fig. 4(d)]. Comparing the AF spectra of the three MFS3 subpopulations with the AF spectra belonging to MFS1 and MFS2, the correspondence appeared evident among the secondary peaks characterizing the different MFS3 subpopulations and those observed in MFS1 and MFS2 [Figs. 4(c) and 4(d)]. The most important difference concerning the intensity ratios between controls and MFS patients was observed in the 445/600- and 520/600-nm ratios: both significantly decreased, but the change was particularly important in the former one (Table 3).

All together, these features indicated a marked increase in lipopigment content, probably joined with a slight increase in oxidized flavins. Therefore, a common feature was the increased emission in the 500 to 700-nm range, which can be explained considering two aspects. First is the increased number and dimensions of autofluorescent granules. It is known that the granule content shows that AF emission peaked at about 540-nm or longer wavelength.[15] Granules seem to colocalize with lysosomes,[27] and their accumulation has been found in transformed fibroblasts[15] as well as in fibroblasts from patients affected by neurological disorders.[28] Second is the highly significant decrease of the AF intensity ratios 445/600 and 520/600, joined with a slight decrease of both the 445/520 and 465/520 ratios, evidenced in all the spectra of MFS fibroblasts and suggesting an increase in oxidized flavins and a marked accumulation of oxidation products such as lipofuscines, which is particularly important in the most seriously ill patient. The differences among the AF spectra of the three MFS3 subpopulations could be due to different intracellular amounts of the various oxidized products: when one of them is much more concentrated than the others, the corresponding emission peak hides the peaks of the other compounds.

Table 3 AF intensity ratios for control and MFS3 cell subpopulations.

Ratio (wavelength, nm)	Control	MFS3 (a)	MFS3 (b)	MFS3 (c)
445/465	1.01±0.04	1.09±0.02	1.04±0.06	1.03±0.03
445/520	1.45±0.15	1.4±0.1	1.20±0.35	1.60±0.15
465/520	1.45±0.08	1.32±0.08	1.10±0.25	1.53±0.09
445/600	4.0±0.5	3.45±0.35	3±1	2.7±0.8
520/600	2.7±0.15	2.4±0.1	2.5±0.1	1.7±0.4

4 Conclusion

In conclusion, fibroblasts from patients with inherited connective tissue disorders showed AF patterns and spectra different from those of the controls. This indicates that AF-based techniques, such as MIAM and AMS, may be utilized to distinguish normal from pathological cells by comparison of their AF spectra and imaging.

It is interesting that fibroblasts from patients affected by very different diseases such as TAA and UCMD showed similar AF emissions, corresponding to similar alterations in the cell energy metabolism and particularly the significant increase of the anaerobic component. Instead, patients with MFS showed peculiar features in the AF spectrum. The differences found between MFS3 and the other MFS patients suggested a correlation between AF emission and the seriousness of the illness. While the three disorders are mainly associated to different genes (TAA is associated to FBN1 in only 5% of cases), all three MFS patients carry mutations in the FBN1 gene.

As we reported, no mutations were found in the TAA patients, which presented a clinical phenotype associated to at least four genes, but probably to others still unknown. Following these results, we cannot exclude the presence of some common genes underlying connective tissue disorders such as UCMD and TAA.

As regards the differences noticed in the MFS patients, the fact that monogenic disorders (one major gene) present mutations in other correlated genes-proteins that are silent when present alone but can act as modifiers of the clinical phenotype when present with a mutation in a major gene is already well known and reported in the literature. The increased AF emission in the 500 to 700-nm range displayed by MFS3 in comparison with MFS1 and MFS2, associated to a more severe and different cardiovascular phenotype, may suggest the presence of important modifier genes in the MFS3 patient.

Overall, in all the connective tissue disorders examined, alterations of cell spreading and cell energy metabolism have been noticed. Moreover, we know that connective tissue disorders are characterized by a defective extracellular matrix (ECM) and, consequently, by defective cell-matrix interactions. In this context, the presence of unknown mutations may be hypothesized in genes encoding for molecules related to major metabolic pathways and/or to the matrix-integrins-cytoskeleton system. However, the latter alone could be enough to cause both metabolic and structural alterations. It is well known that a defective microtubule network may lead to an impairment of the mitochondrial function and, in turn, may trigger apoptosis via intrinsic pathways.[29]

To the best of our knowledge, this is the first time that the AF properties of fibroblasts in primary cultures from patients affected by connective tissue diseases have been studied. These studies may indicate a new diagnostic tool in connective inherited pathologies, although a large number of patients will be required to better evaluate the potential role of AF analysis in clinical and differential diagnosis.

Acknowledgments

This work was partially supported by grants from Italian MIUR (PRIN Project No. 2005064770) and from Ente Cassa di Risparmio di Firenze.

References

1. B. Loeys, L. Nuytinck, I. Delvaux, S. De Bie, and A. De Paepe, "Genotype and phenotype analysis of 171 patients referred for molecular study of the fibrillin-1 gene FBN1 because of suspected Marfan syndrome," *Arch. Intern Med.* **161**, 2447–2454 (2001).
2. G. Matyas, E. Arnold, T. Carrel, D. Baumgartner, C. Boileau, W. Berger, and B. Steinmann, "Identification and *in silico* analyses of novel TGFBR1 and TGFBR2 mutations in Marfan syndrome–related disorders," *Hum. Mutat.* **27**, 760–769 (2006).
3. K. K. Singh, K. Rommel, A. Mishra, M. Karck, A. Haverich, J. Schmidtke, and M. Arslan-Kirchner, "TGFBR1 and TGFBR2 mutations in patients with features of Marfan syndrome and Loeys-Dietz syndrome," *Hum. Mutat.* **27**, 770–777 (2006).
4. T. Mizuguchi, G. Collod-Beriubd, T. Akiyama, M. Abifadel, N. Harada, T. Morisaki, D. Allard, M. Varret, M. Claustres, H. Morisaki, M. Ihara, A. Kinoshita, K. Yoshiura, C. Junien, T. Jajii, G. Jondeau, T. Ohta, T. Kishino, Y. Furukawa, Y. Nakanura, N. Niikawa, C. Boileau, and N. Matsumoto, "Heterozygous TGFBR2 mutations in Marfan syndrome," *Nat. Genet.* **36**, 855–860 (2004).
5. H. Pannu, V. T. Fadulu, J. Chang, A. Lafont, S. N. Hasham, E. Sparks, P. F. Giampietro, C. Zaleski, A. L. Estrera, H. J. Safi, S. Shete, M. C. Willing, C. S. Raman, and D. M. Milewicz, "Mutations in transforming growth factor-beta receptor type II cause familial thoracic aortic aneurysms and dissections," *Circulation* **112**, 513–520 (2005).
6. H. Pannu, V. Tran-Fadulu, and D. M. Milewicz, "Genetic basis of thoracic aortic aneurysms and aortic dissections," *Am. J. Med. Genet.* **139**, 10–16 (2005).
7. O. Camacho Vanegas, E. Bertini, R. Z. Zhang, S. Petrini, C. Minosse, P. Sabatelli, B. Giusti, M. L. Chu, and G. Pepe, "Ullrich scleroatonic muscular dystrophy is caused by recessive mutations in collagen type VI," *Proc. Natl. Acad. Sci. U.S.A.* **98**, 7516–7521 (2001).
8. T.-C. Pan, R.-Z. Zhang, D. G. Sudano, S. K. Marie, C. G. Bonnemann, and M. L. Chu, "New molecular mechanism for Ullrich congenital muscular dystrophy: a heterozygous *in frame* deletion in the COL6A1 gene causes a severe phenotype," *Am. J. Med. Genet.* **73**, 355–369 (2003).
9. E. Bertini and G. Pepe, "Collagen type VI and related disorders: Bethlem myopathy and Ullrich scleroatonic muscular dystrophy," *Eur. J. Paediatr. Neurol.* **6**, 193–198 (2002).
10. B. Giusti, L. Lucarini, V. Pietroni, S. Lucioli, B. Bandinelli, P. Sabatelli, S. Squarzoni, S. Petrini, C. Gartioux, B. Talim, F. Roeles, L. Merlini, H. Topaloglu, E. Bestini, P. Guicheney, and G. Pepe, "Dominant and recessive Col6A1 mutations in Ullrich scleroatonic muscular dystrophy," *Ann. Neurol.* **58**, 400–410 (2005).
11. F. Fusi, G. Agati, M. Monici, R. Pratesi, S. Romano, and P. A. Bernabei, "Multicolor imaging autofluorescence microscopy: a new technique for the discrimination of normal and neoplastic tissues and cells," in *Recent Research Developments in Photochemistry and Photobiology*, S. G. Pandalai, Ed., pp. 79–93, Transworld Research Network, Trivandrum, India (2002).
12. H. Stübel, "Die fluorezenz tierischer gewebe in ultravioletten licht," *Pfluegers Arch. Gesamte Physiol. Menschen Tiere* **142**, 1–14 (1911).
13. W. A. Carrington, R. M. Lynch, E. D. Moore, G. Isenberg, K. E. Fogarty, and F. S. Fay, "Superresolution three-dimensional images of fluorescence in cells with minimal light exposure," *Science* **268**, 483–487 (1995).
14. M. Monici, "Cell and tissue autofluorescence research and diagnostic application," *Biotechnol. Annu. Rev.* **11**, 227–256 (2005).
15. A. C. Croce, A. Spano, D. Locatelli, S. Barni, L. Sciola, and G. Bottiroli, "Dependence of fibroblasts autofluorescence properties on normal and transformed conditions. Role of metabolic activity," *Photochem. Photobiol.* **69**, 364–374 (1999).
16. B. R. Masters and B. Chance, "Redox confocal imaging: intrinsic fluorescent probes of cellular metabolism," in *Fluorescent and Luminescent Probes for Biological Activity*, W. T. Matson, Ed., pp. 44–56, Academic, London (1993).
17. D. C. Wallace, "Mitochondrial diseases in man and mouse," *Science* **283**, 1482–1493 (1999).
18. H. Andersson, T. Baechi, M. Hoechl, and C. Richter, "Autofluorescence of living cells," *J. Microsc.* **191**, 1–7 (1998).
19. G. P. Connolly, "Fibroblast models of neurological disorders: fluorescence measurement studies," *Trends Pharmacol. Sci.* **19**, 171–177 (1998).

20. G. Bearman and R. Levenson, "Biological imaging spectroscopy," in *Biomedical Photonics Handbook*, T. Vo-Dinh, Ed., chr. 8, pp. 1–25, CRC Press, Boca Raton, FL (2003).
21. G. Pepe, E. Bertini, B. Giusti, T. Brunelli, P. Comeglio, B. Saitta, L. Merlini, M. L. Chu, G. Federici, and R. Abbate, "A novel *de novo* mutation in the triple helix of the COL6A3 gene in a two-generation Italian family affected by Bethlem myopathy. A diagnostic approach in the mutation's screening of type VI collagen," *Neuromuscul Disord.* **258**, 264–271 (1999).
22. G. Pepe, B. Giusti, E. Bertini, T. Brunelli, B. Saitta, P. Comeglio, A. Bolognese, L. Merlini, G. Federici, R. Abbate, and M. L. Chu., "A heterozygous splice site mutation in COL6A1 leading to an in-frame deletion of the alpha1(VI) collagen chain in an Italian family affected by Bethlem myopathy," *Biochem. Biophys. Res. Commun.* **258**, 802–807 (1999).
23. A. De Paepe, R. B. Devereux, H. C. Dietz, R. C. M. Hennekam, and R. E. Pyeritz, "Revised diagnostic criteria for the Marfan syndrome," *Am. J. Med. Genet.* **62**, 417–426 (1996).
24. J. E. Aubin, "Autofluorescence of viable cultured mammalian cells," *J. Histochem. Cytochem.* **27**, 36–43 (1979).
25. N. Sitte, K. Merker, T. Grune, and T. von Zglinicki, "Lipofuscin accumulation in proliferating fibroblasts *in vitro*: an indicator of oxidative stress," *Exp. Gerontol.* **36**, 475–486 (2001).
26. D. E. Ingber, "The architecture of life," *Sci. Am.* **278**, 48–57 (1998).
27. E. Goldin, E. J. Blanchette-Mackie, N. K. Dwyer, P. G. Pentchev, and R. O. Brady, "Cultured skin fibroblasts derived from patients with mucolipidosis 4 are auto-fluorescent," *Pediatr. Res.* **37**, 687–692 (1995).
28. M. J. Bennett, S. F. Poirier, L. Chern, A. R. Gayton, G. P. Hosking, N.-A. Le, S. Majumdar, and H. M. Korchak, "Juvenile neuronal ceroid-lipofuscinosis: characterization of the dyslipoproteinaemia and demonstration of membrane phospholipid and phospholipid-dependent signal transduction abnormalities in cultured skin fibroblasts," *J. Inherit Metab. Dis.* **16**, 308–311 (1993).
29. H. Schatten, M. L. Lewis, and A. Chakrabarti, "Spaceflight and clinorotation cause cytoskeleton and mitochondria changes and increases in apoptosis in cultured cells," *Acta Astronaut.* **49**, 399–418 (2001).